Mössbauer investigations and molecular orbital calculations on epidote

Article *in* Physics and Chemistry of Minerals · January 2001

DOI: 10.1007/s002690100150

3 authors, including:

Soraya Heuss-Aßbichler
Ludwig-Maximilians-University of Munich
62 PUBLICATIONS **1,001** CITATIONS

SEE PROFILE

Georg Amthauer
University of Salzburg
513 PUBLICATIONS **3,336** CITATIONS

SEE PROFILE

Phys Chem Minerals (2001) 28: 675–681

ORIGINAL PAPER

M. Grodzicki · S. Heuss-Assbichler · G. Amthauer

Mössbauer investigations and molecular orbital calculations on epidote

Received: 13 November 2000 / Accepted: 16 May 2001

Abstract The electronic structure of iron-rich epidote has been investigated by cluster molecular orbital calculations in local spin density approximation. Calculated quadrupole splittings for Fe(III) at both the M1 and M3 sites are in quantitative agreement with the experimental values obtained by Mössbauer spectroscopy. A detailed analysis of the theoretical results shows that a strong tetragonal compression of the M3 octahedron is responsible for the unusually large value of the quadrupole splitting of Fe^{M3}(III). The corresponding electric field gradient (efg) is dominated by the anisotropy of the valence shell of iron, whereas the ligands contribute only about 15% to the efg. The calculations emphasize that rather large clusters, extending beyond the second coordination sphere of iron, are necessary for a reliable description. Small clusters including only the first coordination sphere of iron generally yield misleading results due to unsaturated oxygen bonds and relatively large cluster charges.

Key words Epidote · Mössbauer spectroscopy · Molecular orbital calculations

Introduction

Members of the epidote group are widespread in low- to medium-grade metamorphic rocks such as calcsilicate rocks, skarns, rodingites, and metabasites. The stability field of epidotes ranges from conditions characteristic of low-pressure hydrothermal systems to significantly higher-pressure environment. Additionally, epidotes may occur as primary phase in calc-alkaline igneous rocks. They consist primarily of the solid solution series between the end members clinozoisite $Ca_2[Al_2Al]Si_3O_{12}OH$ and pistacite $Ca_2[Fe_2Fe]Si_3O_{12}OH$. In general, the amount of Fe(III) is restricted to 1.05 Fe per formula unit (pfu). Monoclinic members up to 0.5 Fe pfu are commonly called clinozoisite, and those with more than 0.5 Fe pfu, epidote.

The crystal structure of epidote was first solved by Ito (1950) for an iron-rich species, and subsequently confirmed in detail by various X-ray investigations of other intermediate members of the series clinozoisite-epidote (Belov and Rumanova 1953; Ito et al. 1954; Dollase 1971; Gabe et al. 1973; Carbonin and Molin 1980; Stergiou et al. 1987; Bonazzi and Menchetti 1995), as well as by neutron diffraction (Nozik et al. 1978; Kvick et al. 1988). All the epidotes studied so far crystallize in the monoclinic space group $P2_1/m$ with two formula units per unit cell, and can be represented by the general formula $A_2M_3Si_3O_{12}OH$. The A sites are occupied by large cations such as Ca, Sr or rare earth elements with high coordination numbers. The three different octahedral M sites generally contain trivalent cations such as Al, Fe(III), Mn(III), etc. Two of the octahedra (M1 and M2) have point symmetry $\bar{1}$ and form chains of edge-sharing octahedra parallel to the crystallographic *b* axis (cf. Fig. 1). These chains are laterally linked by SiO_4 tetrahedra and Si_2O_7 double tetrahedra to a ring. The octahedral M2 site, as the smallest and most regular site, is occupied exclusively by Al. The M3 octahedra are attached on alternate sides to the chain of the M1 octahedra along its length so that one M3 octahedron shares common edges with two different M1 octahedra. The M3 site has point symmetry *m* and is the largest and most distorted site (Stergiou et al. 1987). The first Mössbauer study of epidote (Bancroft et al. 1967) showed that Fe(III) preferentially occupies the distorted M3 site. This result was later confirmed by neutron

Dedicated to Prof. E.-G. Jäger, Jena, on the occasion of his 65th birthday

M. Grodzicki (✉) · G. Amthauer
Institute of Mineralogy, University of Salzburg,
Hellbrunner Str. 34, 5020 Salzburg, Austria
Fax: +43-662-8044622
e-mail: michael.grodzicki@sbg.ac.at

S. Heuss-Assbichler
Institute of Mineralogy and Petrography,
University of Munich, Theresienstr. 41,
80333 Munich, Germany

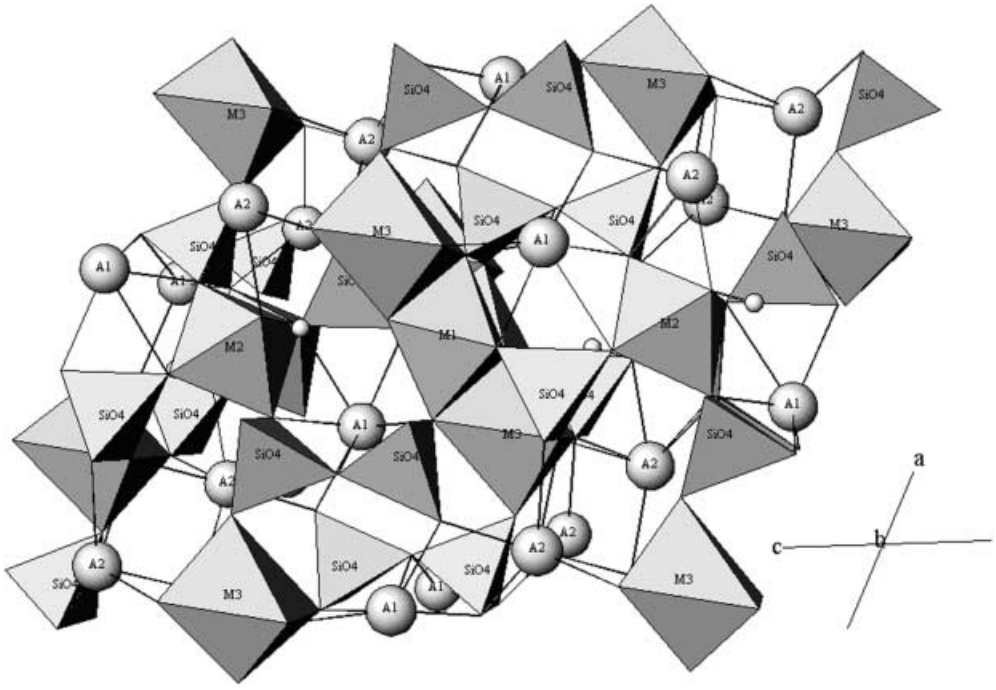

Fig. 1 The structure of epidote (space group $P2_1/m$)

diffraction measurements (Nozik et al. 1978; Kvick et al. 1988) and other Mössbauer studies (Dollase 1973; Bird et al. 1988; Patrier et al. 1991; Artioli et al. 1995; Fehr and Heuss-Assbichler 1997). Fe(III) on the M1 site has not been detected in epidotes with iron content below about 0.75 Fe pfu (Dollase 1973; Fehr and Heuss-Assbichler 1997), but in iron-rich epidotes, small amounts of Fe(III) may enter into the M1 position, where the intracrystalline exchange $Al \rightleftharpoons Fe(III)$ between the M1 and M3 sites may be described by a nonconvergent ordering process (Bird and Helgeson 1980). Finally, Mössbauer spectroscopy, as well as magnetic susceptibility measurements, indicate that Fe(III) is in a high-spin electronic state (Burns and Strens 1967).

The Mössbauer spectra of epidotes (cf. Fig. 2) exhibit two peaks of equal intensity. In addition, iron-rich samples with more than 0.75 Fe pfu may exhibit an inner shoulder, indicating the existence of a second doublet. While the isomer shifts δ of both doublets with values of 0.36 mm s^{-1} are similar and characteristic of Fe(III), their quadrupole splittings ΔE_Q are distinctly different. All Mössbauer spectra yield values between 1.89 and 2.06 mm s^{-1} (sign has not been determined) for the dominant doublet that has uniformly been assigned to Fe(III) in the more distorted M3 site (Bancroft et al. 1967; Dollase 1973; Bird et al. 1988; Patrier et al. 1991; Artioli et al. 1995; Fehr and Heuss-Assbichler 1997). Such a quadrupole splitting is unusually large for high-spin ferric iron in approximately octahedral coordination. On the other hand, the experimentally determined values for the quadrupole splitting of the less intense doublet in iron-rich epidotes, that is attributed to Fe(III) in the more regular M1 site, varies

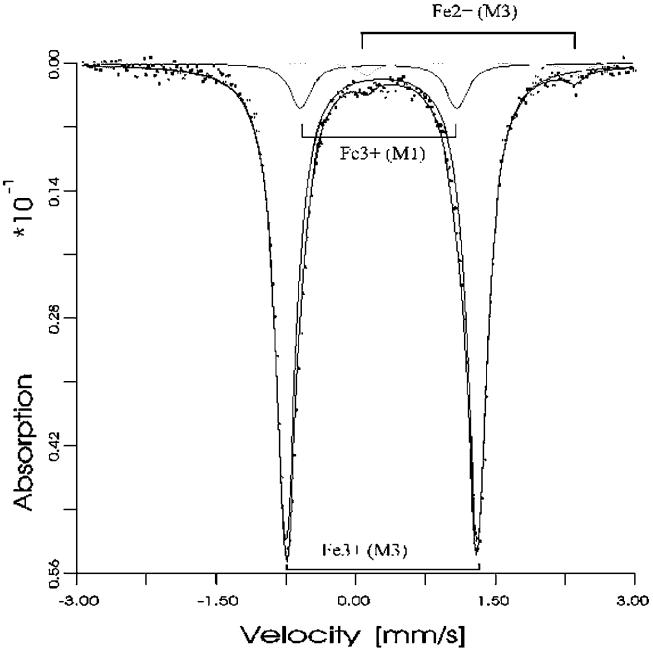

Fig. 2 Mössbauer spectrum of an iron-rich epidote (0.98 Fe pfu) taken at 298 K absorber temperature. (After Fehr and Heuss-Assbichler 1997)

considerably between 1.33 mm s^{-1} (Dollase 1971), 0.80–1.00 mm s^{-1} (Patrier et al. 1991), 0.97 mm s^{-1} (Artioli et al. 1995), and 1.50–1.62 mm s^{-1} (Fehr and Heuss-Assbichler 1997). Although this variation may be caused by structural differences, it seems more likely to be due to uncertainties in evaluating the measured spectra because of the low Fe occupation of the M1

site. Minor amounts of Fe(II) that have also been detected can easily be identified by their isomer shift values in the range between 1.10 and 1.31 mm s^{-1} (Fehr and Heuss-Assbichler 1997).

The purpose of the present study is to understand the unusually large quadrupole splitting of Fe(III) in the M3 octahedra, as well as the difference between the M3 site value and that for the M1 site. Preliminary investigations on Fe^{M3}(III) have demonstrated the capability of electronic structure calculations to reproduce at least qualitatively the measured spectra (Grodzicki et al. 1999). In this paper, extensive cluster molecular orbital (MO) calculations have been carried out in local spin density approximation for a series of clusters with varying size for the M1 and M3 site, respectively. In the next section the theoretical basis of these calculations is briefly outlined, followed by a detailed description of the various model clusters. Afterwards, the theoretical results are presented and analyzed in detail in order to elucidate the close connection between the geometrical and electronic structure.

Theoretical methods

All calculations have been performed in local spin density approximation (LSDA) by the spin-polarized self-consistent charge (SCC) $X\alpha$ method (Grodzicki 1980, 1985). However, the $X\alpha$ potential (with $\alpha = 0.7$) is used only for the evaluation of the two- and three-center integrals, while the one-center integrals are derived from all-electron (relativistic) atomic Dirac-Fock calculations. Furthermore, the core electrons enter the two- and three-center integrals via a pseudopotential also derived from relativistic atomic calculations. The method is hence ab initio in the sense that it does not contain any adjustable parameter. The calculation of hyperfine parameters within the framework of a valence-electron-only MO method has been described in detail previously (Grodzicki et al. 1987). In particular, the evaluation of the electric field gradient (efg) tensor $V_{\alpha\beta}$ is based on dividing the charge density into the positive point charges Q_μ^{core} of the ionic cores and the charge distribution arising from the valence electrons:

$$V_{\alpha\beta} = \sum_{\mu\neq 0} Q_\mu^{\text{core}} \hat{V}_{\alpha\beta}(\vec{R}_{\mu 0}) - e_0 \sum_{\mu\nu ij} P_{ij}^{\mu\nu} \int \varphi_i^\mu(\vec{r}-\vec{R}_{\mu 0}) \hat{V}_{\alpha\beta}(\vec{r}) \varphi_j^\nu(\vec{r}-\vec{R}_{\nu 0}) d^3r$$

The iron atom is located at $\vec{R}_0, \vec{R}_{\mu 0} = \vec{R}_\mu - \vec{R}_0, e_0$ is the (positive) elementary charge, $P_{ij}^{\mu\nu}$ the bond-order matrix, $\varphi_i^\mu(\vec{r})$ is the i-th atomic orbital at the μ-th atom, and the tensor operator components $\hat{V}_{\alpha\beta}(\vec{r})$ are given as

$$\hat{V}_{\alpha\beta}(\vec{r}) = \frac{1-\gamma(r)}{r^3} \frac{3r_\alpha r_\beta - r^2\delta_{\alpha\beta}}{r^2} \quad ,$$

where the Sternheimer shielding function $\gamma(r)$ arises from the polarization of the core electrons of the iron atom by charges outside the core and has been derived from atomic self-consistent first-order perturbation calculations (Lauer et al. 1979). With respect to a basis set of atomic orbitals, the efg tensor can be decomposed into three different contributions according to the location of the atomic orbitals in the matrix elements:

1. Valence contribution with both atomic orbitals at the iron site, i.e.:

$$V_{\alpha\beta}^{\text{val}} = -e_0 \sum_{ij} P_{ij}^{00} \int \varphi_i^0(\vec{r}) \hat{V}_{\alpha\beta}(\vec{r}) \varphi_j^0(\vec{r}) d^3r \quad .$$

The radial part of the remaining one-center integral is proportional to $\langle r^{-3}\rangle(1-R)$, where the Sternheimer antishielding constant R has the value 0.075 (Lauer et al. 1979), and the expectation value $\langle r^{-3}\rangle$ is derived from relativistic atomic calculations as a function of the valence shell occupation.

2. Covalence contribution with one atomic orbital at the iron site and the other one at a ligand atom, i.e.:

$$V_{\alpha\beta}^{\text{cov}} = -e_0 \sum_{vij} P_{ij}^{0\nu} \int \varphi_i^0(\vec{r}) \hat{V}_{\alpha\beta}(\vec{r}) \varphi_j^\nu(\vec{r}-\vec{R}_{\nu 0}) d^3r \quad ,$$

that describes the anisotropy of the electron distribution within the iron-ligand bonds.

3. Ligand contribution with both atomic orbitals at ligand atoms, i.e.:

$$V_{\alpha\beta}^{\text{lig}} = \sum_{\mu\neq 0} Q_\mu^{\text{core}} \hat{V}_{\alpha\beta}(\vec{R}_{\mu 0}) - e_0 \sum_{\mu\nu ij} P_{ij}^{\mu\nu} \int \varphi_i^\mu(\vec{r}-\vec{R}_{\mu 0}) \hat{V}_{\alpha\beta}(\vec{r}) \varphi_j^\nu(\vec{r}-\vec{R}_{\nu 0}) d^3r \quad ,$$

where the sum in the electronic part runs over all ligands, i.e., $\mu, \nu \neq 0$. In this case, the Sternheimer shielding function $\gamma(r)$ can be replaced with γ_∞ having a value of -8.70 (Lauer et al. 1979). It should be emphasized that this definition is not identical to the common use of this term in crystal-field or point-charge approximations. The evaluation of all integrals has been described in detail elsewhere (Grodzicki et al. 1987).

The measured quadrupole splitting, ΔE_Q, is related to the components $|V_{zz}| \geq |V_{yy}| \geq |V_{xx}|$ of the electric field gradient (efg) tensor in its principal axes system by:

$$\Delta E_Q = (1/2) e Q V_{zz} (1 + \eta^2/3)^{1/2} \quad ,$$

where the asymmetry parameter $\eta = (V_{xx} - V_{yy})/V_{zz}$ describes the deviation from axial symmetry. The size of the nuclear quadrupole moment Q of the first excited state of ^{57}Fe is assumed to be 0.15 barn (Ray and Das 1977; Lauer et al. 1979). In the principal axes system of the efg tensor, the efg V_{zz} is simply the sum of the valence, covalence and ligand contribution, as described above. The valence part is roughly proportional to the anisotropies

$$\Delta n_d = n_{x^2-y^2} + n_{xy} - n_{z^2} - (n_{xz} + n_{yz})/2$$
$$\Delta n_p = (n_x + n_y)/2 - n_z$$

of the Fe(3d) shell and Fe(4p) shell occupations, respectively. Usually, the anisotropy of the Fe(3d) shell dominates the efg for high-spin ferrous iron, whereas it is generally assumed that for high-spin ferric iron the ligand contribution should be the largest.

Model clusters

The construction of the subsequent model clusters starts from the most recent low-temperature (15 K) neutron diffraction data of a natural iron-rich epidote with 0.76 Fe pfu and cell parameters $a = 8.893$ Å, $b = 5.630$ Å, $c = 10.150$ Å, $\beta = 115.36°$ (Kvick et al. 1988). The first coordination sphere of the most distorted Fe^{M3}(III) exhibits not just a substantial tetragonal compression along the O_4–O_8 axis taken as the z axis with distances of 1.8601 and 1.9435 Å, but also considerably different Fe–O distances of 1.9871 and 2.2164 Å to the four (equatorial) oxygens, resulting in a ratio of 0.90 between the average axial and equatorial bond distances. The octahedra of the M1 site are less distorted, with similar equatorial Fe–O distances of 1.9407 and 1.9566 Å, and smaller distances of 1.8454 Å to the axial O_4 oxygens, resulting again in a tetragonal compression, though less pronounced, with an axial to equatorial ratio of 0.95. Three model clusters of different size have been investigated in detail for the M3 site. The smallest one, $[Fe^{M3}(III)O_6]^{9-}$ (model 1), represents just the first coordination sphere of iron. In the next step, a cluster was constructed that

includes all polyhedra of those cations bonded to the six oxygens of the first coordination sphere. These comprise two edge-sharing M1 octahedra and five corner-sharing SiO_4 tetrahedra. Terminating the cluster at the oxygens of these polyhedra yields, however, an inappropriate description of the charge distribution and of the electronic properties. First of all, the formal oxygen charge of -2 results in a large negative cluster charge that causes convergence problems if not compensated by a Madelung-type potential, e.g., by appropriately distributed point charges. Secondly, omitting the outer cations bonded to the terminal oxygens produces unsaturated O(2*p*)-lone-pair orbitals that are in the same energy range as the Fe(3*d*) orbitals and may occasionally also cause convergence problems. Actually, both the bonding to the omitted cations and the Madelung potential will lead to a stabilization of these O(2*p*) orbitals and thus would remove the convergence problems. While this stabilization can be attained, of course, by adding further polyhedra, though at the expense of CPU time and memory space, earlier experience (Lougear et al. 2000) has shown that the effect of these polyhedra can be simulated with sufficient accuracy either by replacing some or all oxygens of the third shell with fluorine atoms, or by terminating them with one or two hydrogens in the direction of the next cations. Both together will reduce the cluster charge and will shift the ligand 2*p* orbitals into the energy range typical for saturated O(2*p*) orbitals. Such a procedure on one hand keeps the size of the clusters manageable and, on the other hand, provides a suitable model for the first coordination sphere of the central iron atom. The resulting cluster has the composition $[Fe^{M3}(III)O_6Al_2Si_5F_{20}]^{3-}$ (model 2) and contains 141 valence orbitals and 213 valence electrons. Finally, the two Ca(II) cations with the shortest Ca–O bond distances are added, viz. Ca_1 bonded to the two O_1 atoms ($d = 2.47$ Å) and Ca_2 bonded to the two O_2 atoms ($d = 2.54$ Å), respectively. Ca_1 is already fivefold-coordinated, so that adding the closest bound anion at $d = 2.296$ Å is sufficient, whereas Ca_2 is only twofold-coordinated. Addition of a single F atom, replacing an O_7 at a distance of 2.251 Å to Ca_2, yields a strong covalent Ca_2–F bond with an unreasonably small charge at this calcium atom, but adding the corresponding Si tetrahedron removes this artifact. The resulting (neutral) cluster (cf. Fig. 3) with the composition $Fe^{M3}(III)O_6Al_2Si_6Ca_2F_{25}$ (model 3) comprises 42 atoms, 173 valence orbitals, and 253 valence electrons, and provides a reasonable description of the environment of the six oxygens of the first coordination sphere. This will later be seen by comparison with larger clusters up to 66 atoms.

The coordinate system has been chosen to coincide with the calculated main axes of the electric field gradient (see below). The *z* axis is oriented along the O_4–O_8 axis and the equatorial oxygens of the first coordination sphere are located close to the bisectors of the *x* and *y* axes. Accordingly, the low-lying t_{2g}-like orbitals comprise the $d_{x^2-y^2}$, d_{xz} and d_{yz} orbitals, while the e_g-like orbitals are d_{z^2} and d_{xy}. The M1 site is modeled by a cluster of five edge-sharing octahedra, together with the adjacent SiO_4 tetrahedra, and the four nearest calcium atoms. Replacing the terminal oxygens by fluorines, the resulting cluster has the composition $[Fe^{M1}(III)O_6Al_4O_8Si_{10}Ca_4F_{34}]^{1+}$ and comprises 273 valence orbitals and 389 valence electrons.

Theoretical results

In order to assess the reliability of the theoretical approach and the suitability of the various model clusters, calculated quadrupole splittings are first compared with the respective experimental data. Afterwards, the electron and spin density distribution is analyzed in detail and utilized to understand the unusually large value of the quadrupole splitting, as well as the differences between the M3 and M1 sites.

The calculated quadrupole splittings at the M3 site for the three model clusters summarized in Table 1 show

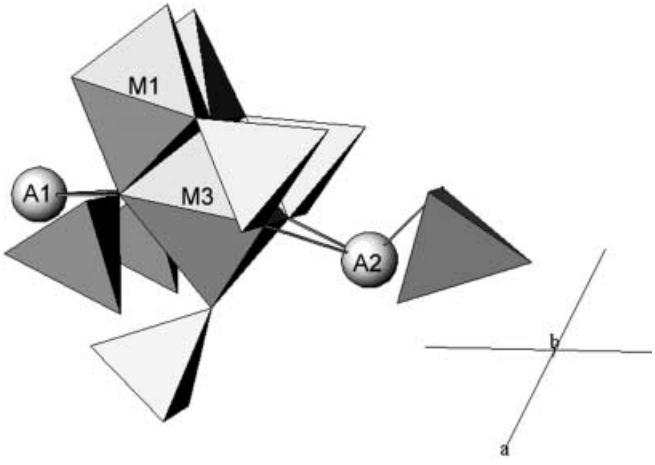

Fig. 3 Sketch of model cluster 3 for the M3 site comprising the central M3 octahedron, two edge-sharing M1 octahedra, five corner-sharing silicon tetrahedra, and two Ca cations (*A*1, *A*2) with a single silicon tetrahedron

Table 1 Calculated quadrupole splitting (in mm s^{-1}), asymmetry parameter η, and efg contributions for the three models of the M3 site. Measured quadrupole splittings vary between 1.89 and 2.06 mm s^{-1} (sign has not been determined)

Model	ΔE_Q	η	Val(3*d*)	Val(4*p*)	Coval	Ligand
1	−1.23	0.45	−0.07	−0.07	−0.46	−0.63
2	−1.45	0.27	−0.69	−0.12	−0.45	−0.19
3	−1.91	0.08	−0.75	−0.25	−0.58	−0.33

that only model 3 yields satisfactory results, with -1.91 mm s^{-1} assuming a nuclear quadrupole moment $Q(^{57}Fe) = 0.15$b. Thus, the calculated absolute value of the quadrupole splitting falls in the range between 1.89 and 2.06 mm s^{-1} of the measured values, and is distinctly larger than the quadrupole splitting usually observed for high-spin ferric iron in approximately octahedral coordination. Increasing the cluster size by including more distant polyhedra yields similar quadrupole splittings of -1.90, -1.84, and -1.93 mm s^{-1} for clusters of 50, 56, and 66 atoms, respectively. Hence, it can be concluded that the electronic structure of iron is at least qualitatively correctly described by model 3. The electric field gradient (efg) is negative, almost axially symmetric with $\eta = 0.08$, and is oriented close to the axial Fe(III)–O_4 bond at an angle of 1.8°. In order to understand the reason for the large quadrupole splitting, the efg is decomposed with respect to its principal axes system into the valence, covalence, and ligand contribution as described above. Within the framework of ligand-field theory, the anisotropy of the Fe(3d) shell

$$\Delta n_d = n_{x^2-y^2} + n_{xy} - n_{z^2} - (n_{xz} + n_{yz})/2$$

will be zero, since each of the five 3*d* orbitals is singly occupied. This has led to the general conclusion that the efg in ferric high-spin compounds arises predominantly from the ligand contribution, and has been taken as the

justification for the applicability of point charge models for calculating the efg tensor in such cases.

The result of the MO calculation for model 3 is obviously at variance with this conclusion (cf. Table 1). The valence contribution turns out to be the largest part, whereas the ligands contribute only about 15% to the total efg, which is even less than the covalence contribution. That such a result is not specific for ferric iron in epidote is demonstrated by recent results for other iron-bearing compounds (Keutel et al. 1999; Grodzicki and Amthauer 2000), where the valence contribution also dominates the efg even though the *d*-shell anisotropy vanishes according to ligand-field theory. In addition, all contributions have a negative sign, indicating an accumulation of charge in the *z* direction. Analyzing first the valence contribution, i.e., the Fe(3*d*) shell anisotropy, it is seen from the last two rows of Table 2 that the spin-up electrons (upper row) yield a negligible anisotropy Δn_d, so that they do not contribute to the efg. This reflects the near-spherical symmetry of the charge distribution of a closed shell as provided by the spin-up 3*d* electrons. Accordingly, the valence part of the efg arises primarily from the covalent admixtures of the formally empty spin-down 3*d* orbitals to the occupied ligand molecular orbitals. The negative sign of Δn_d is mainly due to the increased occupation of the $3d_{z^2}$ orbital, corresponding to a larger covalent mixing of this spin-down orbital with the occupied ligand molecular orbitals that is caused by the shorter bond distances between iron and O_4 and O_8, respectively, compared with the equatorial $Fe^{M3}(III)$–O_1 and $Fe^{M3}(III)$–O_2 bond lengths. Similarly, the negative 4*p*-shell contribution shows that the $4p_z$ orbital undergoes stronger covalent interaction than the $4p_x$ and $4p_y$ orbitals.

The small ligand contribution, as well as the comparatively large covalence contribution, can be understood by analyzing the charge distribution within the first coordination sphere of iron, as given in Table 3 (last row). First, the average effective charge of the axial oxygens is nearly equal to the average charge of the equatorial oxygens, so that the ligand contribution of the first coordination sphere arises predominantly from the different bond length. A rough estimate of $V_{zz}^{\mathrm{lig}} \propto 4Q(^{57}\mathrm{Fe})(1-\gamma_\infty)\bar{Q}_{\mathrm{av}}(\bar{R}_{\mathrm{eq}}^{-3}-\bar{R}_{\mathrm{ax}}^{-3})$ yields the small value of -0.23 mm s^{-1} in qualitative agreement with the exactly calculated value for model cluster 3. On the other hand, the considerable differences in the overlap populations between the axial and equatorial Fe–O bonds give rise to the comparatively large covalence contribution. Altogether, the pronounced charge anisotropy in the *z* direction is responsible for the large quadrupole splitting, and reflects the strong tetragonal compression of the M3 octahedron.

Comparing next the results for the three model clusters, the quadrupole splitting is seen to be rather sensitive with regard to the cluster size (Table 1). Whereas the value of -1.91 mm s^{-1} for model cluster 3 is within the range of the experimental values, both of the smaller model clusters yield considerable deviations from this value. In the case of model 1, the main difference is the strong negative ligand contribution due to the cluster charge of -9 a.u., leading to the high oxygen charges between -1.55 and -1.77 a.u. (Table 3). Moreover, the valence contributions from the Fe(3*d*) and Fe(4*p*) shells are an order of magnitude smaller, so that the result for this model seems to confirm the expectations derived from simple ligand field theory. Model cluster 2 does not exhibit these anomalies, but all contributions are uniformly about one third too small compared with model 3, mainly for two reasons. First, the total charge of cluster 2 is -3 a.u., while cluster 3 is neutral. Second, the two Ca atoms included in model 3 but not in model 2 are located approximately in the *xy* plane, i.e. they are bound to the equatorial oxygens. Therefore, they give a negative ligand contribution to the efg and, via a moderate covalent interaction [overlap populations $P(Ca_1O_1)$ and $P(Ca_2O_2)$ are 0.11 and 0.22, respectively] with the equatorial oxygens, they also influence the 3*d* shell occupation of iron by reducing, e.g., the occupation numbers of the $3d_{xy}$ and $3d_{x^2-y^2}$ orbitals that are primarily determined by the interaction with the equatorial oxygens. Altogether, the calculations demonstrate that even the moderately strong Ca–O orbital interactions with Ca–O bond distances of 2.47 and 2.54 Å, respectively, may influence the electric field gradient at the iron atom. On the other hand, adding the two more remote Ca atoms coordinated to O_8 (bond distance 3.03 Å) and to O_2 (bond distance 2.80 Å), as well as increasing the

Table 2 Occupation numbers and *d*-shell anisotropy Δn_d of the spin-up and spin-down 3*d*-shell of $Fe^{M3}(III)$ for the three model clusters

Model	$n_{x^2-y^2}$	n_{xz}	n_{yz}	n_{xy}	n_{z^2}	Δn_d
1-up	0.998	0.993	0.996	0.991	0.982	0.013
1-down	0.160	0.220	0.200	0.267	0.262	−0.046
2-up	0.998	0.995	0.996	0.990	0.975	0.018
2-down	0.105	0.281	0.154	0.224	0.338	−0.226
3-up	0.998	0.996	0.996	0.985	0.972	0.015
3-down	0.048	0.217	0.151	0.204	0.337	−0.269

Table 3 Effective charges *Q*, overlap populations *P*, *d*-shell occupation *n* and *d*-shell spin density *m* of $Fe^{M3}(III)$ for the three model clusters

	Q(Fe)	$Q(O_4)$	$Q(O_8)$	$Q(O_2)$	$Q(O_1)$	$P(FeO_4)$	$P(FeO_8)$	$P(FeO_2)$	$P(FeO_1)$	$n(3d)$	$m(3d)$
1	0.984	−1.615	−1.545	−1.637	−1.774	0.247	0.302	0.202	0.121	6.071	3.851
2	1.150	−0.520	−0.464	−0.459	−0.457	0.275	0.258	0.176	0.072	6.057	3.852
3	0.809	−0.456	−0.414	−0.441	−0.437	0.349	0.395	0.233	0.106	5.905	3.991

cluster size further by inclusion of more distant polyhedra, does not improve the results, as mentioned above.

In addition, several other geometries of epidotes with iron contents between 0.60 and 0.86 Fe pfu have been tested in order to explore the effect of the accompanying geometrical changes on the efg. The calculated quadrupole splittings vary only slightly with -1.95 mm s^{-1} (0.60 Fe pfu, Stergiou et al. 1987), -1.89 mm s^{-1} (0.75, Nozik et al. 1978), -1.92 mm s^{-1} (0.84, Gabe et al. 1973), -1.91 mm s^{-1} (0.86, Carbonin and Molin 1980, sample CAL), and -2.09 mm s^{-1} (Dollase 1971, allanite). These results demonstrate that a regular expansion of the first coordination sphere of Fe^{M3} has virtually no influence on the quadrupole splitting that is roughly determined by the extent of the tetragonal compression as expressed by the ratio between the axial and equatorial bond distances. This ratio is close to 0.90 in all cases.

In some iron-rich epidotes (Fig. 2), another ferric doublet has been detected and assigned to Fe(III) in the more regular M1 site, as well as a weak ferrous doublet that has been assigned to Fe(II) in the M3 octahedron (Patrier et al. 1991; Fehr and Heuss-Assbichler 1997). The reliable calculation of the corresponding hyperfine parameters suffers from uncertainties in the geometrical parameters because replacing Al with Fe(III) (M1 site) or Fe(III) with Fe(II) (M3 site) will be accompanied by local distortions of the coordination sphere of iron. As far as a regular expansion of the octahedron is concerned, the influence on the quadrupole splitting will be minor, but anisotropic distortions may cause some changes. Since it is difficult to estimate the extent of such distortions, quantitative accuracy cannot be expected, but qualitative trends should be reflected in the calculations. A necessary, but of course not sufficient, criterion for a reliable geometry is the condition that iron should remain in the (observed) high-spin state. This condition is fulfilled for Fe^{M1}(III), i.e., the intermediate-spin state ($S = 3/2$) and the low-spin state ($S = 1/2$) are located 0.196 and 1.822 eV, respectively, above the high-spin state. The calculated quadrupole splitting of -1.30 mm s^{-1} falls into the range of the experimental values, and is thus considerably smaller than the one obtained for the M3 site. The reason for this reduced quadrupole splitting is the smaller anisotropy $\Delta n_d = -0.121$ of the Fe(3d) shell, which is only half as large as for the M3 site, mainly due to an increase in the occupation numbers of the spin-down $3d_{xy}$ and $3d_{x^2-y^2}$ orbitals. These increased values arise from the stronger covalent interactions between these orbitals and the equatorial oxygens due to the significantly shorter Fe–O bond distances. Altogether, the calculations supply the theoretical basis for the phenomenological correlation that, for ferric high-spin iron, the absolute value of the quadrupole splitting generally increases with increasing distortion (Burns 1994). This increase is, however, not due to the ligand contribution, but arises from the 3d shell anisotropy.

Analogous calculations made on model 3 for Fe(II) at the M3 site yield, without changing the geometrical parameters, both the intermediate-spin ($S = 1$) and the low-spin state ($S = 0$) higher in energy than the (observed) high-spin ground state by 1.007 and 1.453 eV, respectively. The calculated quadrupole splitting is $+2.03$ mm s^{-1}, while the experimental values vary between 1.78 and 2.38 mm s^{-1} (sign has not been determined). Even when taking into account that some changes in the local geometry are possible on substituting Fe(III) with Fe(II), this value is considerably smaller than the common range of 2.60–3.60 mm s^{-1} for ferrous iron quadrupole splitting in minerals. The reason for this range of values is well understood (Grodzicki and Amthauer 2000; Lougear et al. 2000) since, in most cases, the efg is dominated by the additional spin-down electron residing in an orbital of almost 100% iron character so that this electron alone produces a quadrupole splitting of roughly 4 mm s^{-1}. The contributions from the other four spin-down 3d electrons and the 4p electrons, as well as the covalence and ligand contributions, are an order of magnitude smaller and have the opposite sign, so that they reduce this value by amounts roughly between 0.5 and 1 mm s^{-1}. According to this consideration, the reason for the small quadrupole splitting of Fe(II) at the M3 site in epidote is essentially the same as that for the large value of Fe(III), viz. the strong tetragonal compression. First of all, with respect to the principle axes system of the efg, the occupied spin-down MO is a $3d_{x^2-y^2}$ orbital with 99% Fe character yielding a quadrupole splitting of $+3.97$ mm s^{-1}. Among the four formally empty spin-down 3d orbitals, the $3d_{z^2}$ orbital undergoes the strongest interaction with the ligands, resulting in an occupation number of 0.22 electrons, whereas the other three orbitals have distinctly lower occupations with values between 0.05 and 0.10 electrons. Due to this anisotropy, a negative contribution of -0.63 mm s^{-1} is obtained. Furthermore, the 4p, covalence, and ligand contributions are -0.33, -0.61, and -0.37 mm s^{-1}, respectively, so that the overall reduction of the contribution from the spin-down $3d_{x^2-y^2}$-electron amounts to -1.94 mm s^{-1}. This is about twice as large as usual, and is again caused by the strong tetragonal compression of the M3 octahedron.

Finally, with regard to trends in the thermodynamic properties, it is instructive to examine the bonding modes of iron. Decomposing the Fe–O overlap populations into the contributions from the 4sp, the $3d_{\uparrow}$, and the $3d_{\downarrow}$ orbitals, respectively, shows that the covalent part of the Fe–O bond is almost exclusively determined by the 4sp orbitals (Table 4). The $3d_{\uparrow}$ orbitals yield a small antibonding (negative) contribution corresponding to the fact that both the bonding and the anti-

Table 4 Contributions to the overlap populations of the iron oxygen bond in epidote

	d (Å)	Total	4sp	3$d\uparrow$	3$d\downarrow$
Fe–O_8	1.840	0.395	0.352	−0.058	0.101
Fe–O_4	1.938	0.349	0.251	−0.037	0.135
Fe–O_2	1.985	0.233	0.199	−0.032	0.066
Fe–O_1	2.236	0.106	0.083	−0.009	0.032

bonding spin-up linear combinations of the Fe($3d_\uparrow$) and the O($2p_\uparrow$) orbitals are occupied. Accordingly, the effective contribution of the 3*d* electrons to the bond is an order of magnitude smaller compared with the 4*sp* electrons. Analogous results have been obtained for iron in chlorite (Lougear et al. 2000), garnets (unpublished results), and vivianite (Grodzicki and Amthauer 2000). Although the covalent contribution constitutes a relatively small part of the total Fe–O bond energy of Fe(III) in epidote, these results suggest that a discussion of ligand-field stabilization energies solely in terms of the *d* electrons requires careful justification.

Conclusions

The electronic structure of iron-rich epidotes has been characterized by cluster molecular orbital calculations based on the local spin density approximation. Model calculations on clusters of varying size have shown that rather large clusters extending beyond the second coordination sphere are necessary to obtain results for the hyperfine parameters in agreement with experimental values. Small clusters, including just the first coordination sphere of iron, generally yield misleading results due to unsaturated oxygen bonds and relatively large cluster charges. Accordingly, large cluster charges should be avoided, and at least the coordination sphere of the oxygens bound to the central iron must be reproduced correctly. On the basis of suitable clusters fulfilling these requirements, calculated quadrupole splittings for Fe(III) at both the M1 and M3 sites are in quantitative agreement with the experimental values. A detailed analysis of the theoretical results demonstrates that the anomalously large value for the quadrupole splitting of Fe^{M3}(III) can be traced back to the strong tetragonal compression of the M3 octahedron. In spite of the formally closed-shell configuration of high-spin Fe(III), the efg is dominated by the valence shell anisotropy of iron, whereas the ligands contribute merely about 15% to the efg.

Acknowledgements This research is funded by the Austrian Fonds zur Förderung der wissenschaftlichen Forschung (FWF), grant no. P12424-GEO. All calculations were carried out at the Research Institute of Software Technology (RIST) in Salzburg.

References

Artioli G, Quartieri S, Deriu A (1995) Spectroscopic data on coexisting prehnite–pumpellyite and epidote–pumpellyite. Can Mineral 33: 67–75

Bancroft GM, Maddock AG, Burns RG (1967) Application of the Mössbauer effect to silicate mineralogy I. Iron silicates of known crystal structure. Geochim Cosmochim Acta 31: 2219–2246

Belov NV, Rumanova IM (1953) The crystal structure of epidote $Ca_2Al_2FeSi_3O_{12}(OH)$. Dokl Akad Nauk SSSR 89: 853–856

Bird DK, Helgeson HC (1980) Chemical interaction of aqueous solutions with epidote-feldspar mineral assemblages in geologic systems I. Thermodynamic analysis of phase relations in the system $CaO–FeO–Fe_2O_3–Al_2O_3–SiO_2–H_2O–CO_2$. Am J Sci 281: 576–614

Bird DK, Cho M, Janik CJ, Liou JG, Caruso LJ (1988) Compositional, order/disorder, and stable isotope characteristics of Al–Fe epidote, State 2–14 drill hole, Salton Sea geothermal system. J Geophys Res 93, B11: 13135–13144

Bonazzi P, Menchetti S (1995) Monoclinic members of the epidote group: effects of the $Al \rightleftharpoons Fe^{3+} \rightleftharpoons Fe^{2+}$ substitution and of the entry of REE^{3+}. Mineral Petrol 53: 133–153

Burns RG (1994) Mineral Mössbauer spectroscopy: correlations between chemical shift and quadrupole splitting parameters. Hyperfine Int 91: 739–745

Burns RG, Strens RGJ (1967) Structural interpretation of polarized absorption spectra of the Al–Fe–Mn–Cr epidotes. Mineral Mag 36: 204–226

Carbonin S, Molin G (1980) Crystal-chemical considerations on eight metamorphic epidotes. N Jb Miner Abh 139: 205–215

Dollase WA (1971) Refinement of the crystal structures of epidote, allanite and hancockite. Am Mineral 56: 447–464

Dollase WA (1973) Mössbauer spectra and iron distribution in the epidote-group minerals. Z Kristallogr 138: 41–63

Gabe EJ, Portheine JC, Whitlow SH (1973) A reinvestigation of the epidote structure: confirmation of the iron location. Am Mineral 58: 218–223

Grodzicki M (1980) A self-consistent-charge Xα method. J Phys (B)13: 2683–2692

Grodzicki M (1985) Theorie und Anwendungen der Self-Consistent-Charge-Xα Methode. Habilitation Thesis, Institute of Theoret Physics, Hamburg 1985

Grodzicki M, Amthauer G (2000) Electronic and magnetic structure of vivianite: cluster molecular orbital calculations. Phys Chem Miner 27: 694–702

Grodzicki M, Männing V, Trautwein AX, Friedt JM (1987) Calibration of isomer shifts and quadrupole coupling constants for ^{119}Sn, ^{127}I and ^{129}I as derived from SCC-Xα calculations and Mössbauer measurements. J Phys B20: 5595–5625

Grodzicki M, Heuss-Assbichler S, Amthauer G (1999) ^{57}Fe Mössbauer spectra and electronic structure of Fe^{3+} in epidote $Ca_2FeAl_2Si_3O_{12}OH$. International Conference Applications of the Mössbauer effect (ICAME99), contribution T6/19, Garmisch-Partenkirchen 1999

Fehr KT, Heuss-Assbichler S (1997) Intracrystalline equilibria and immiscibility along the join clinozoisite-epidote: an experimental and ^{57}Fe Mössbauer study. N Jb Miner Abh 172: 43–67

Ito T (1950) X-ray studies on polymorphism, Chap. 5. Maruzen C, Tokyo

Ito T, Morimoto N, Sadanaga R (1954) On the structure of epidote. Acta Crystallogr 7: 53–59

Keutel H, Käpplinger I, Jäger EG, Grodzicki M, Schünemann V, Trautwein AX (1999) Structural, magnetic and electronic properties of a pentacoordinated intermediate-spin ($S = 3/2$) iron(III) complex with a macrocyclic $[N_4]^{2-}$ ligand. Inorg Chem 38: 2320–2327

Kvick A, Pluth JJ, Richardson JW, Smith JV (1988) The ferric ion distribution and hydrogen bonding in epidote: a neutron diffraction study at 15 K. Acta Cryst (B)44: 351–355

Lauer S, Marathe VR, Trautwein AX (1979) Sternheimer shielding using various approximations. Phys Rev (A)19: 1852–1861

Lougear A, Grodzicki M, Bertoldi C, Trautwein AX, Steiner K, Amthauer G (2000) Mössbauer and molecular orbital study of chlorites. Phys Chem Miner 27: 258–269

Nozik YZ, Kanepit VN, Fukin LY, Makarov YS (1978) A neutron diffraction study of the structure of epidote. Geochem Intern 15(2): 66–69

Patrier P, Beaufort D, Meunier A, Eymery JP, Petit S (1991) Determination of the nonequilibrium ordering state in epidote from the ancient geothermal field of Saint Martin: application of Mössbauer spectroscopy: Am Mineral 75: 602–610

Ray SN, Das TP (1977) Nuclear quadrupole interaction in the Fe^{2+} ion including many-body effects. Phys Rev (B)16: 4794–4804

Stergiou AC, Rentzeperis PJ, Sklavounos S (1987) Refinement of the crystal structure of a medium iron epidote. Z Kristallogr 178: 297–305